COMPDYN 2013
4th ECCOMAS Thematic Conference on
Computational Methods in Structural Dynamics and Earthquake Engineering
M. Papadrakakis, N.D.Lagaros, V. Plevris (eds.)
Kos Island, Greece, 12–14 June 2013

WIND CHARACTERISTICS AROUND AND EFFECTS ON A SEA-CROSSING BRIDGE BASED ON MONITORING DATA

Limin SUN[1], Yi ZHOU[1], and Zhihua MIN[2]

[1] State Key Laboratory for Disaster Reduction of Civil Engineering, Tongji University
Siping Rd. 1239, Shanghai, 200092, P.R.China
lmsun@tongji.edu.cn

[2] College of Civil Engineering, Shanghai Normal University
Haisi Rd. 100, Fengxian, Shanghai, 201418, P.R.China
zhmin_tj@hotmail.com

Keywords: Wind Environment, Wind Induced Vibration, Structural Health Monitoring, Cable-Stayed Bridge.

Abstract. *Wind loading is critical for a long-span and flexible bridge under operation. This paper studied the wind loading on a sea-crossing bridge, namely the Main Navigational Channel Bridge (MNCB) of Donghai Bridge at Shanghai, utilizing the field measurement data from its Structural Health Monitoring System (SHMS). Located at the typhoon prone area off the eastern coast of China, the instrumented bridge is a five-span cable-stayed bridge arranged as 73+132+420+132+73m, with a three-cell steel-concrete composite box girder. In this paper, first of all, based on the data of wind speed and direction monitored by two anemometers, one on the mid-span of girder and the other on one tower's tip, the wind environment at the bridge site during the period from January 2007 to December 2012 is summarized in terms of the 10-min mean wind speed, mean wind direction, turbulence intensities and so on. Then, the extreme wind environment during strong winds, e.g. typhoons, and the strong-wind-induced structural responses, such as accelerations, are investigated by statistical analysis. Finally, the influence of strong winds on the variation of the bridge's modal frequency and damping ratio is discussed. During the high winds, modal frequencies become more scattered while damping ratios have an increasing trend. This research could serve as a field measurement basis for wind-resistance design and evaluation of long-span bridges in similar environments.*

1 INTRODUCTION

Wind is one of dominant loads for the large-span, light-weighted and flexible structures. Focused on the cable supported long-span bridges, the wind resistant evaluation, whether in the design stage or in the operation stage, is desired in the view of safety, serviceability and durability. As is quite well known, on the other hand, full-scale measurement of civil structures becomes more and more common, especially with the booming of Structural Health Monitoring campaigns around the world. [1-12] A well-developed SHM system could provide a huge database of recorded environmental conditions and structural responses, which has two attractive features, say, on-site and full-scale, compared with the results from numerical simulation and wind tunnel experiments. Although field measurement inevitably suffers from both the large uncertainty from unknown/uncontrolled factors and the limited measurement points due to the budgets, long-term and even continuously recorded data are still invaluable and much suitable to perform statistical analysis for the validation of or feed-back to the design theories and assumptions. As a result, more and more researches have been conducted about the wind characteristics and its effects on the stay cables, bridge girders and so on, based on the field measurements. [13-17]

The current paper presents two topics, i.e. wind environment and wind's effects, in summary form, processing the data from SHMS installed on the MNCB of Donghai Bridge over a period of 6 years. The former topic explores the statistical characteristics of the overall wind field on-site from 2007 to 2012 and during the strong wind events, which could serve as a field measurement basis for the verification of the wind-resistance design and the subsequent bridge condition evaluation. The latter topic discusses the bridge's acceleration responses and modal parameters' variation during high winds, with an attempt to better understand the responding mechanism of the long-span bridges to wind, as well as to better control the daily traffic conditions.

2 DONGHAI BRIDGE AND ITS SHMS

Located off the China's eastern coast and open to the traffic in Dec. 2005, Donghai Bridge is a vital sea-crossing linkage between Luchao Port at Shanghai City and the Yangshan Deepwater Port with a total length of over 32.5km (Figure 1). One of the key portions of this transport artery is the Main Navigational Channel Bridge (MNCB), a five-span cable-stayed bridge arranged as 73+132+420+132+73m. Its girder is a three-cell composite box girder, consisting of steel bottom flange and webs, and prestressed high-performance concrete top flange, with a width/depth ratio of 33m/4m=8.25. Twinned stays are arranged in a single plane and the two towers have an inverted Y shape with the designed elevation at top 159m. The MNCB's axis goes with a slightly rotation, about 1°, from the north-south direction in anticlockwise.

In order to optimize the bridge maintenance and ensure the service standard, a Structural Health Monitoring System (SHMS) has come into use since Sep. 2006, which includes 8 monitoring regions and 478 sensors of various kinds measuring the structural static and dynamic responses as well as environmental conditions. [18] The MNCB is the 5th monitoring region and totally 181 sensors were distributed on the girder, pylons and cables (Figures 2 and 3). For example, to accurately measure the horizontal wind on site, the instrumentation system includes two anemometers, one at the top of the northern tower PM335 denoted as 5WS001, the other at the center span of the girder denoted as 5WS002 with 6m away from the midpoint to the north. Both of anemometers have a sampling frequency of 1Hz and a range of wind speed of 0.4m/s ~ 75m/s. The elevations of 5WS001 and 5WS002 are, respectively, 159.50m and 58.15m above the sea level incorporating the sensor's masts.

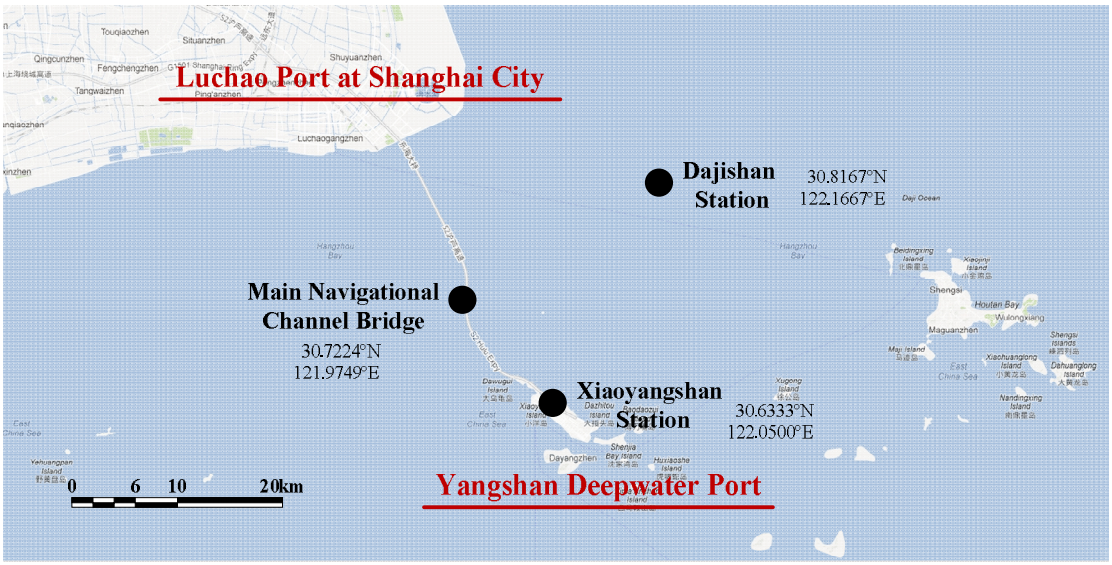

Figure 1: Locations of Measurement Stations and MNCB

In the design stage, this region's wind condition was determined according to the following two meteorological stations nearby, i.e. Dajishan Station (DJS for short) and Xiaoyangshan Station (XYS for short) as shown in Figure 1. DJS is about 21km away from the MNCB at the altitude of 81.00m, while XYS is nearly 12km away from the MNCB at the altitude of 32.90m. [19, 20]

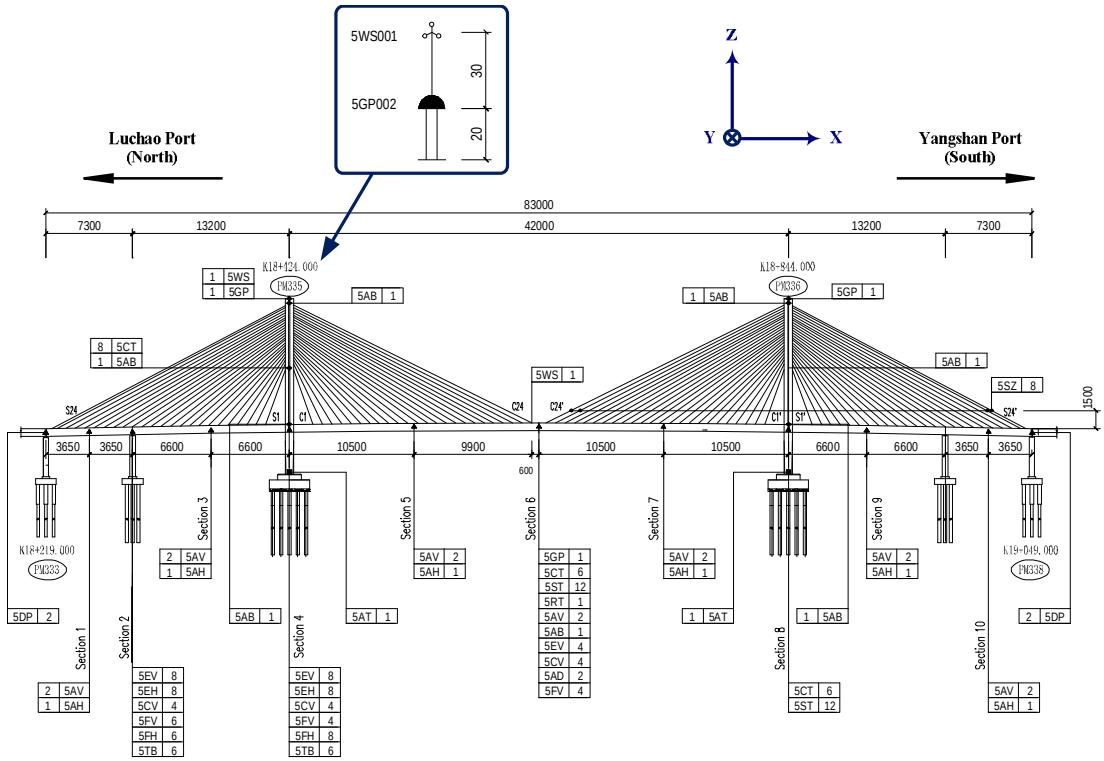

Figure 2: Elevation of the Main Navigational Channel Bridge (Unit: cm; 5EV/5CV/5EH-Strain Gauge; 5SZ-Cable Force; 5GP-GPS Station; 5AV/5AH/5AB/5AT/5AD-Accelerometer; 5FV/5FH-Fatigue Sensor; 5WS-Weather Station; 5DP-Extensometer; 5ST/5RT/5CT/5TB-Thermometer)

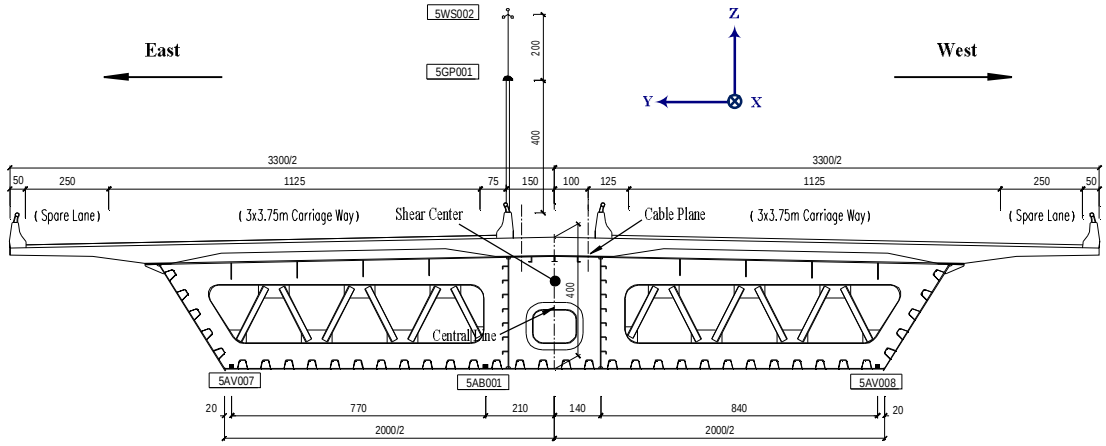

Figure 3: Section View of the MNCB (Unit: cm)

The MNCB's modes regarding the center span of the girder within 0~5 Hz are listed in Table 1, and the 1st vertical bending mode, the 1st lateral bending mode and the 1st torsional mode of the MNCB are plotted in Figure 4.

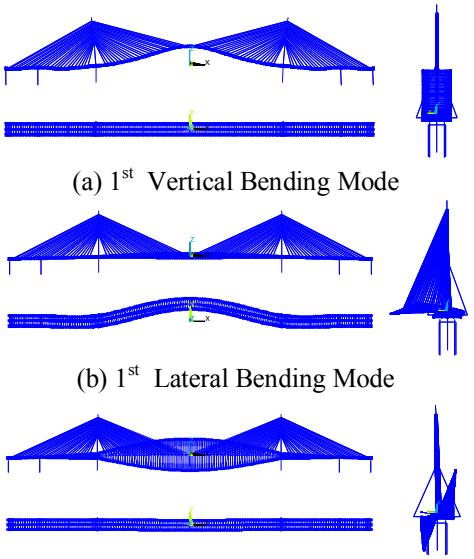

(a) 1st Vertical Bending Mode

(b) 1st Lateral Bending Mode

(c) 1st Torsional Mode

Figure 4: 1st Vert./Lat./Tor. Modes

Mode (Description)	Freq. (Hz)	Mode (Description)	Freq. (Hz)
Mode # (Vert. #)		**Mode # (Lat. #)**	
2 (Ver. 1)	0.361	3 (Lat. 1)	0.434
4 (Ver. 2)	0.513	13 (Lat. 2)	1.245
8 (Ver. 3)	0.778	26 (Lat. 3)	2.282
9 (Ver. 4)	1.013	54 (Lat. 4)	3.919
14 (Ver. 5)	1.378	77 (Lat. 5)	5.425
17 (Ver. 6)	1.694	**Mode # (Tor. #)**	
22 (Ver. 7)	2.042	5 (Tor. 1)	0.635
31 (Ver. 8)	2.662	12 (Tor. 2)	1.186
40 (Ver. 9)	3.113	21 (Tor. 3)	2.030
49 (Ver. 10)	3.593	30 (Tor. 4)	2.497
57 (Ver. 11)	4.145	38 (Tor. 5)	3.013
65 (Ver. 12)	4.602	53 (Tor. 6)	3.890
71 (Ver. 13)	4.954	58 (Tor. 7)	4.243
Mode # (Long. #)		64 (Tor. 8)	4.593
1 (Long. 1)	0.206	70 (Tor. 9)	4.857
29 (Long. 2)	2.497		
61 (Long. 3)	4.416		

Table 1: Modes of Center Span within 0~5Hz

3 OVERALL WIND CHARACTERISTICS DURING 6 YEARS

The records of wind speed and wind direction from 2007-1-1 to 2012-12-31 are retrieved and processed through the conventionally vector-decomposition based method [21] with the averaging period 10 minutes, thus obtaining the 10-min mean wind speed $\overline{U}$ and the fluctuating components at longitudinal and lateral direction, u and v. After excluding the data over the periods when the monitoring system failed, the statistics of the 6 years wind field are computed from approximately 270000 10-min records at the deck level, and about 230000 10-min records at the tower-top level.

3.1 Wind frequency during 6 years

Figure 5 displays the wind roses of the mean wind speeds from both tower-top and deck measurements for a comparison with the assumed wind roses in the design stage. The radial distances in the plot represent the percentage of the total number of the 10-min segments from a particular direction. It can be seen that wind directions at tower-top and deck level are dramatically different, which might reflect the Ekman spiral. However more probably, it comes from the interference from the bridge. Furthermore, the wind frequency at the bridge site is significantly different from those at DJS and XYS, which indicates the weak correlation between two spots separated about 20km in this region.

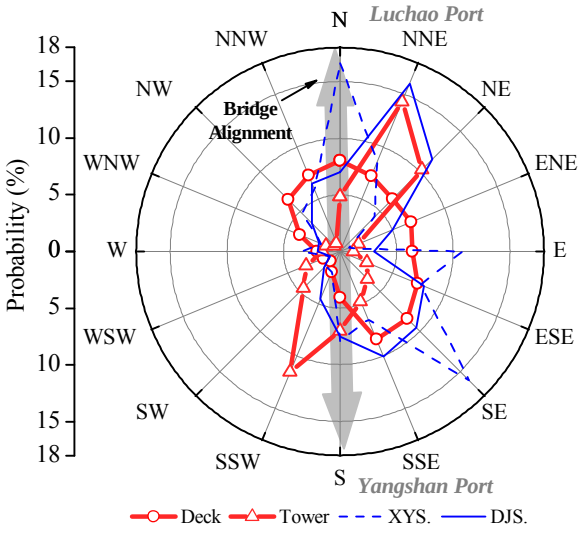

Figure 5: Wind Frequency Compared with Design

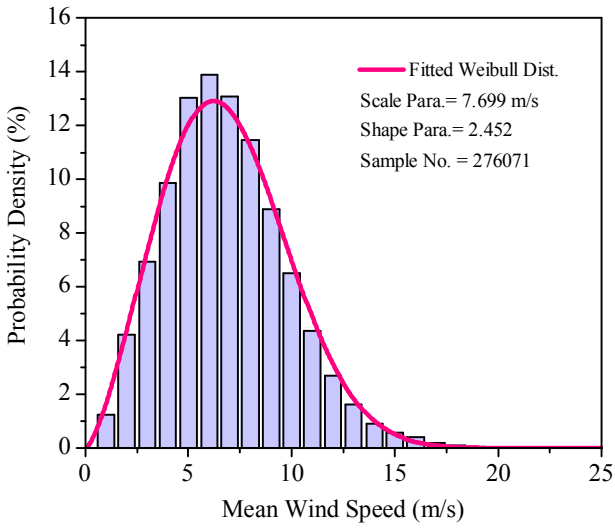

Figure 6: 10-min Mean Wind Speed Histogram

3.2 Mean wind profile

According to the power-law profile, recommended by China's Wind-resistant Design Specification for Highway Bridges [22], the exponent α in (1) is estimated from the 10-min records over the periods when both 5WS001 and 5WS002 are normal.

$$\frac{U_t}{U_d} = \left(\frac{Z_t}{Z_d}\right)^{\alpha} \tag{1}$$

In (1)(2), U and Z respectively represent the 10-min mean wind speed and measurement point's height, while the subscripts t and d denotes tower-top and deck. Given Z_d =58.15m and Z_t =159.50m, then the mean of α is 0.15, which is close to the value corresponding to terrain category B in [22] but larger than α =0.10 in the design manual.

Considering the deck is of more interest in the design and evaluation, only the deck measurement is considered in the following for brevity.

3.3 Mean wind speed distribution

The histogram of 10-min mean wind speed at the deck level is shown in Figure 6, which is in good agreement with the Weibull distribution [23] whose p.d.f. is formulated as (2), and the fitted parameters are 2.452 for the shape parameter k, and 7.699m/s for the scale parameter c.

$$f(x) = \left(\frac{kx^{k-1}}{c^k}\right) \exp\left[-\left(\frac{x}{c}\right)^k\right] \tag{2}$$

3.4 Recurrence of wind field

Figure 7 and 8 are the wind roses of 10-min mean wind and daily maximum mean wind for each year. The style of wind rose here are different from that in Figure 5 in that a tangential length, which is meaningless, is added just for visualization enhancement. The wind speed intervals in Figure 7 and 8 are based on the Beaufort Wind Scale [24] without the height modification. In Figure 7, 0~7.9m/s, 8.0~13.8m/s, ⩾13.8m/s correspond to scale 0~4, scale 5~6, and greater or equal than scale 7; likewise, in Figure 8, 0~13.8m/s, 13.9~17.1m/s, ⩾ 17.2m/s correspond to scale 0~6, scale 7 and greater or equal than scale 8. These two figures show an obvious one-year cycle, which indicates a particular wind distribution pattern does exist at the location of the MNCB and it could be modeled by joint probability density function of wind speed and wind direction. [25]

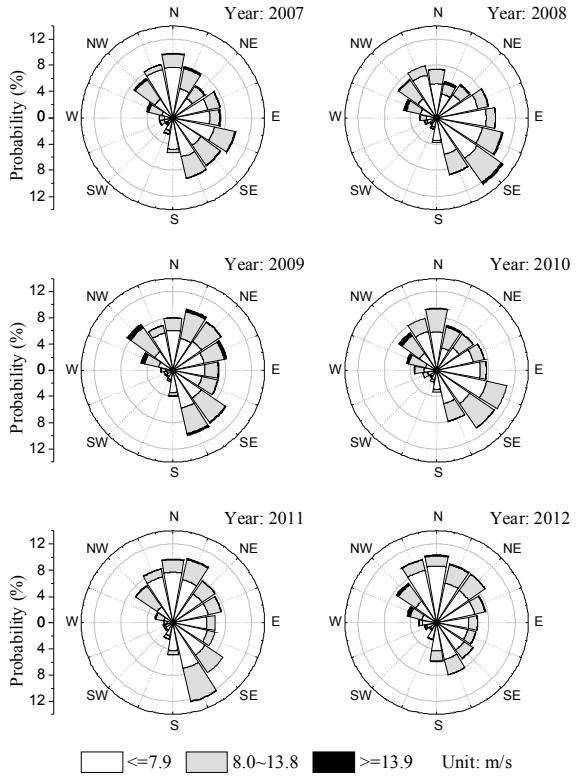

Figure 7: Mean Wind for Each Year

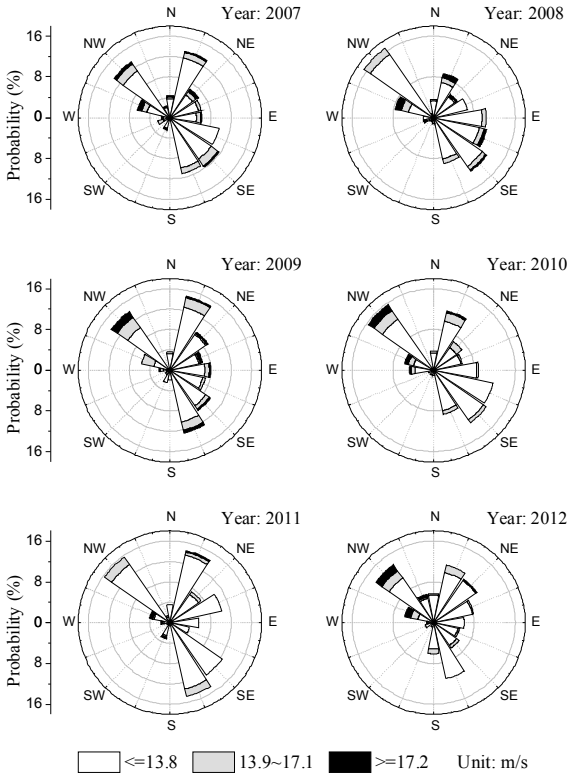

Figure 8: Daily Maximum Wind for Each Year

Further examination on the wind frequency for each season is also performed, which exhibits the characteristics of a subtropical monsoon climate, i.e. wind mainly blowing from southeast in summer and from northwest in winter.

3.5 Characteristics of turbulence components

The variance, turbulence intensity, integral length scale are calculated to characterize the fluctuating components u and v, as listed in the 4th column of Table 2. It is important to point out that in the current paper, all the quantities are computed from 10-min averaging duration following the conventional method, which assumes the wind is stationary in each 10-min segment. The actual wind field during some periods, however, are far from the stationarity,

e.g. during the typhoon Haikui the wind direction changed fiercely (Figure 12). Therefore, the turbulent characteristics are generally overestimated in Table 2, and a more appropriate average time duration is needed for the subsequent research in the near future.

	Formula	Design Value	6 Years	8-22 Gale	Wipha	Krosa	Muifa	Haikui	Bolaven
Time Interval Time1	From ~ To		2007/1/1 0:00 ~ 2013/1/1 0:00	2008/8/22 17:30 ~ 2008/8/22 18:30	2007/9/19 0:00 ~ 2007/9/19 16:00	2007/10/7 14:00 ~ 2007/10/9 8:00	2011/8/6 13:00 ~ 2011/8/7 17:00	2012/8/7 11:00 ~ 2012/8/9 5:00	2012/8/27 0:00 ~ 2012/8/28 0:00
Max. Gust m/s	$\max(U(t))$	–	–	46.40	25.50	33.00	37.00	35.20	30.10
Max. Mean Wind m/s	$\max(\overline{U})$	–	–	23.38	20.38	24.96	26.38	23.81	22.87
Mean Wind $\overline{U}$ (m/s)	$\frac{1}{T}\int_0^T U(t)\,dt$	51	6.828	11.29	16.28	17.14	18.06	10.46	11.30
Variance σ_u^2 (m/s)^2	$\frac{1}{T}\int_0^T u^2(t)\,dt$	–	0.876	40.54	1.73	3.39	5.99	65.77	1.82
Variance σ_v^2 (m/s)^2	$\frac{1}{T}\int_0^T v^2(t)\,dt$	–	0.943	17.21	1.79	3.06	3.55	60.94	1.09
Turb. Int. I_u (%)	$\frac{\sigma_u}{\overline{U}}$	10	13.78	35.35	7.91	10.89	12.53	161.42	14.00
Turb. Int. I_v (%)	$\frac{\sigma_v}{\overline{U}}$	9	14.58	26.50	8.13	10.50	10.48	157.16	12.90
Gust Factor $G_u(t_g)$	$1+\max(u(t_g))/\overline{U}$	1.38	1.299	1.75	1.17	1.23	1.29	3.71	1.34
Gust Factor $G_v(t_g)$	$\max(v(t_g))/\overline{U}$	–	0.295	0.43	0.18	0.22	0.23	3.01	0.29
Integ. Len. L_u^x (m)	$\frac{\overline{U}}{\sigma_u^2}\int_0^{0.05\sigma_u^2} R_u(\tau)\,d\tau$	120	89.079	630.57	154.53	274.30	194.58	159.40	154.98
Integ. Len. L_v^x (m)	$\frac{\overline{U}}{\sigma_v^2}\int_0^{0.05\sigma_v^2} R_v(\tau)\,d\tau$	60	53.093	492.36	48.63	178.70	134.44	204.56	96.48

*Note: u and v denote longitudinal and lateral characteristics respectively; and t_g in Gust Factor is 3s.

Table 2: Wind Characteristics on site

Figure 9 and 10 show the polar plots of the mean values of the turbulence intensities I_u, I_v and integral length scales L_u, L_v versus directions ranging from 0~360° in 22.5° increments at the deck level. It is interesting to note that I_u, I_v on the north and south are greater than those on the other directions, while L_u, L_v on the north and south are smaller than other directions. Both of the above results indicate the wind has stronger turbulence along the bridge axis, which most likely results from the disturbance from the bridge.

4 WIND CHARACTERISTICS DURING STRONG WIND

In this section, wind characteristics during strong wind at the MNCB's site are explored. According to the website [26], there is in total 17 typhoon processes entering the circle with the center at the MNCB and the radius 400km from Jan. 2007 to Dec. 2012, and 5 of them

have an instantaneous wind speed exceeding 25m/s at the deck level, whose tracks were shown in Figure 11. Additionally, the measured highest wind speed at the deck level over 6 years comes from a strong localized gale process occurred on 2008-8-22, which is also picked out for a further discussion.

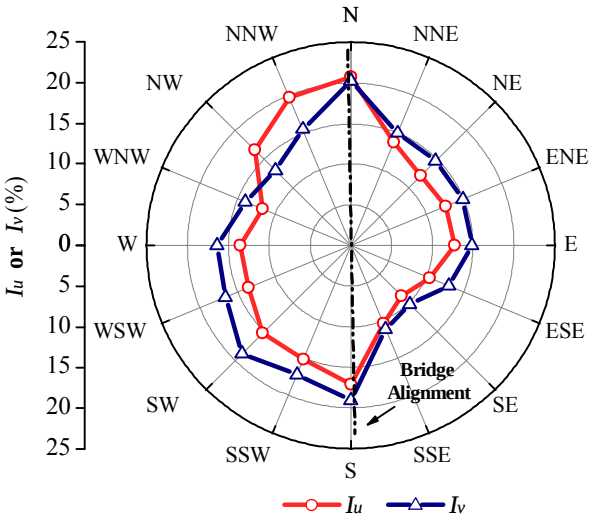

Figure 9: I_u and I_v for Each Direction

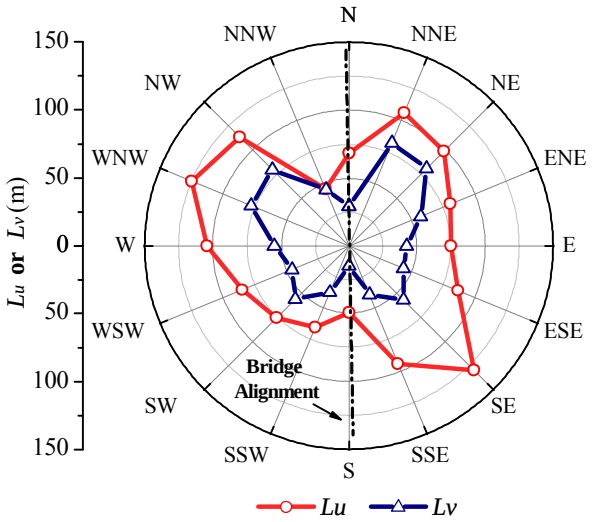

Figure 10: L_u and L_v for Each Direction

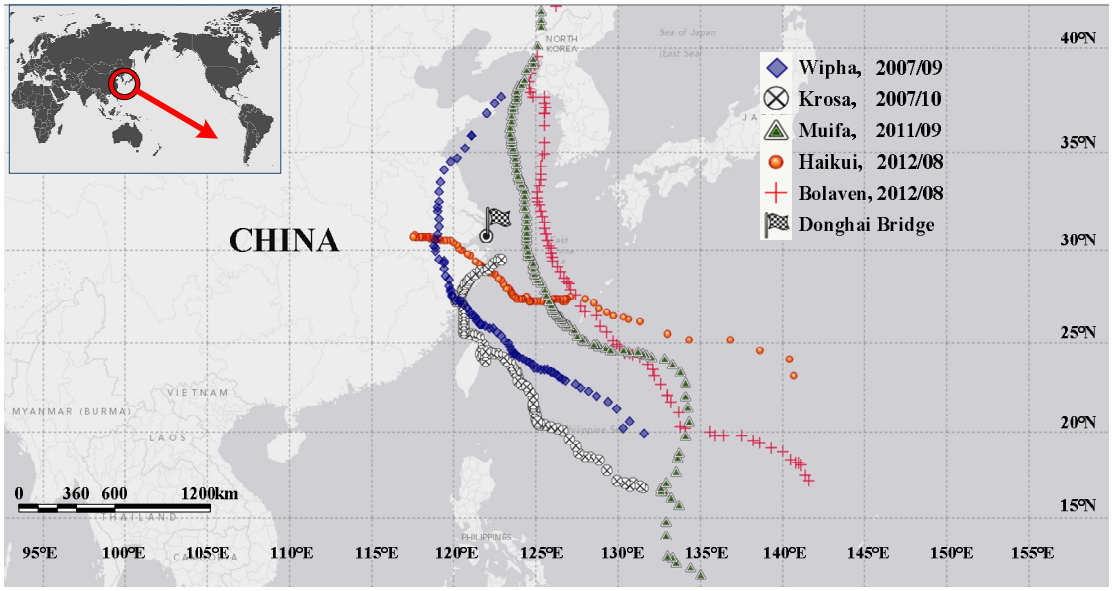

Figure 11: Typhoon Tracks

The measured wind speeds and directions during these 6 strong wind processes are plotted in Figure 12, where the dashed lines indicates the periods when the MNCB is within the typhoon circle with the radius of 15.4m/s for the 5 typhoon processes. Typhoon Haikui is unique because the MNCB is even within the typhoon circle with the radius of 25.7m/s as indicated by the dot and dash lines in Figure 12 (e). Table 2 lists the characteristics of each strong wind which is calculated based on the 10-min average time duration. By comparison with the statistics over 6 years, it can be seen that the turbulent variance σ^2 and the mean wind speed during strong wind processes are consistently larger than those in the ordinary wind field, but the gust factors G, turbulence intensities I and integral length scales L does not ex-

hibit obviously qualitative trend. It should be noted that usually the wind field is non-stationary during strong winds, so the calculated statistics in Table 2 may not reflect the physical characteristics as mentioned above. Preferable are either shorter averaging duration or other methods suitable to model the non-stationary wind field like in [27].

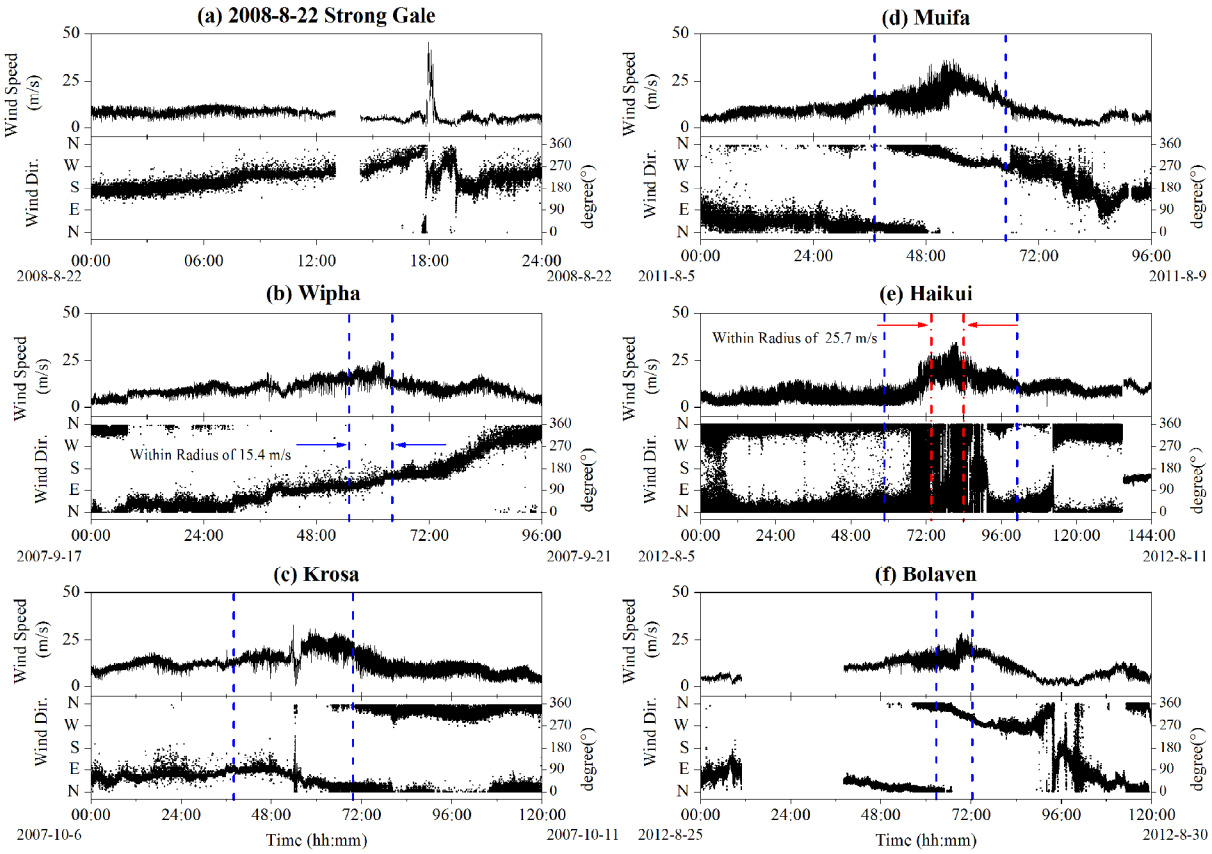

Figure 12: Time Histories of Each Strong Wind

5 STRUCTURAL RESPONSE DURING STRONG WINDS

This paper focuses on the acceleration responses during strong winds at the mid span of girder. As shown in Figure 3, the accelerometers don't reside on the centroid of the cross-section, so the first step is to transform the measured acceleration responses to the vertical, lateral, torsional accelerations $\ddot{V}$、$\ddot{H}$、$\ddot{\alpha}$ regarding to the centroid. Note that the centroid and shear center of the standard cross-section of the MNCB are 1.29m and 1.34m below the top surface, respectively; thus it is acceptable not to distinguish them strictly. The measurement points for the vertical acceleration are $AV007$ and $AV008$, which are 19.6m apart from each other; and for the horizontal acceleration is $AB001$, which is 2.71m below the centroid. The measurement data could be related to $\ddot{V}$、$\ddot{H}$、$\ddot{\alpha}$ as

$$\begin{cases} \ddot{\alpha} \times 9.8 + \ddot{V} = AV007 \\ -\ddot{\alpha} \times 9.8 + \ddot{V} = AV008 \\ \ddot{\alpha} \times 2.71 + \ddot{H} = AB001 \end{cases} \tag{3}$$

Hence,

$$\begin{cases} \ddot{\alpha} = (AV007 - AV008) / (2 \times 9.8) \\ \ddot{V} = (AV007 + AV008) / 2 \\ \ddot{H} = AB001 - 2.71 \times \ddot{\alpha} \end{cases} \tag{4}$$

Figures 13 and 14 are the acceleration time histories at the midspan of the girder during 2008-8-22 gale and Typhoon Haikui. When Haikui hit the MNCB, the bridge was closed to traffic for about 35 hours and this period could be readily identified from Figure 14, indicating the traffic has great impact on the bridge's dynamic response. With closer observation, it is possible to compare the effects of wind and traffic on the acceleration amplitude. For the vertical and torsional acceleration, the traffic loading seems to take more advantages than the wind. Because only the super strong winds like 8-22 Gale and Typhoon Haikui could excite these two accelerations to the same order of magnitude as the traffic loading. However, for the lateral acceleration, the wind loading is so dominant that the maximum magnitude during high wind is many times as that in the normal traffic condition, which is also listed in Table 3.

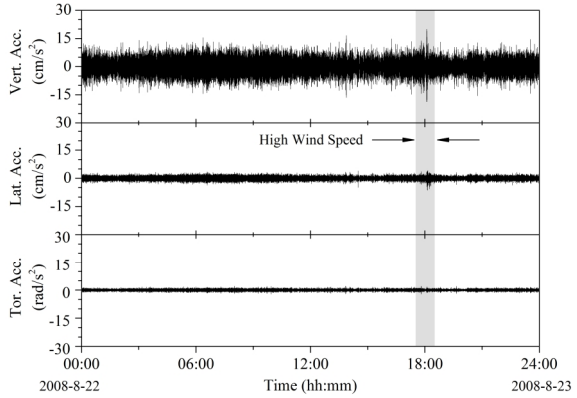

Figure 13: Acceleration on 2008-8-22

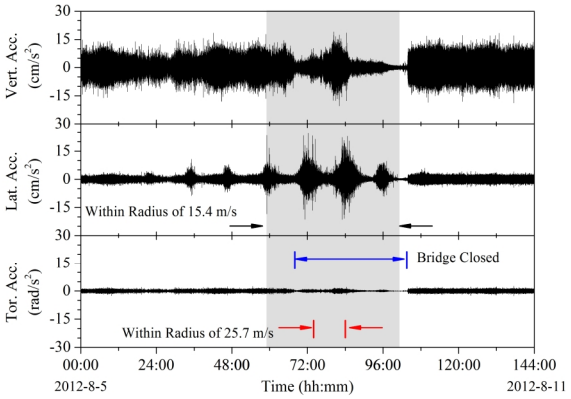

Figure 14: Acceleration during Typhoon Haikui

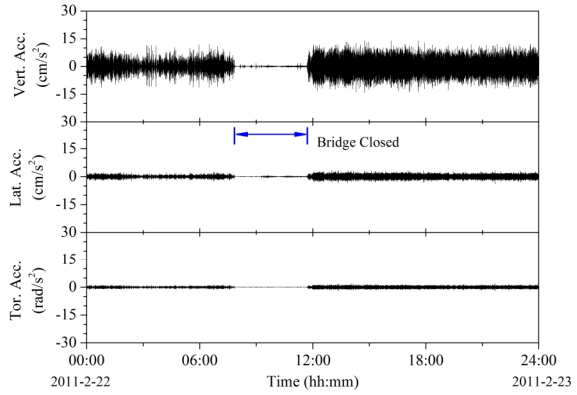

Figure 15: Acceleration on 2011-2-22

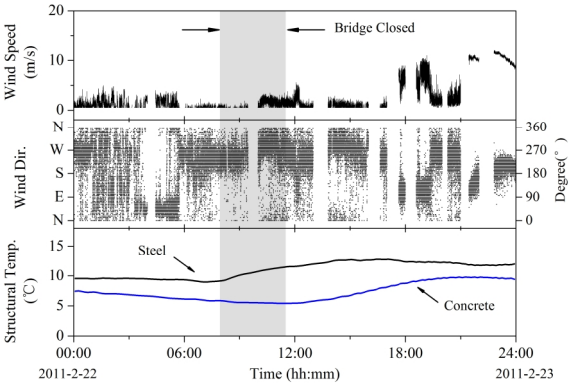

Figure 16: Temp. and Wind Condition on 2011-2-22

In order to investigate the relationship among wind, traffic loading and girder's accelerations, the following four "one-hour" records are selected out, which correspond to four typical cases:

- CASE I: without high wind and without traffic, i.e. 2011-2-22 9:00~10:00;
- CASE II: without high wind but with traffic, i.e. 2011-2-22 5:00~6:00;
- CASE III: with high wind but without traffic, i.e. 2012-8-8 11:00~12:00 during Haikui;

- CASE IV: with high wind and with traffic, i.e. 2008-8-22 17:30~18:30.

On the morning of 2011-2-22, a severe traffic accident happened on the Donghai Bridge, causing the bridge closed for about 4 hours. Figures 15 and 16 present the deck acceleration responses, structural temperatures and wind condition at the tower top (the deck's anemometer is out of work). Fortunately, during the bridge closure the wind is small and temperature is stable, so CASE I could serve as a base-line. By comparing other cases with it, the strong wind and traffic loading's effects could be clear.

			1/2 of the Middle Span				Tower Bot. of PM335		
	Time Interval Time2	Statistics	Vert. Acc. cm/s^2	Lat. Acc. cm/s^2	Tor. Acc. rad/s^2	Long. Acc. cm/s^2	Lat. Acc. cm/s^2	Long. Acc. cm/s^2	Vert. Acc. cm/s^2
8 • 22 Gale	2008/8/22 17:30 ~ 2008/8/22 18:30	Max	19.92	4.14	2.03	2.14	0.39	2.33	1.24
		RMS1*	2.66	0.57	0.27	0.36	0.05	0.21	0.12
	Other	RMS2*	1.91	0.46	0.23	0.30	0.05	0.07	0.05
Typhoon Haikui	2012/8/7 21:00 ~ 2012/8/9 7:00	Max	19.02	24.55	2.18	3.78	1.78	5.24	34.52
		RMS1*	1.81	0.81	0.19	0.24	0.07	0.42	0.42
	Other	RMS2*	2.12	0.56	0.25	0.35	0.06	0.16	0.07
Traffic Accident	2011/2/22 8:00 ~ 2011/2/22 11:00	Max	1.76	0.59	0.22	0.35	0.06	0.22	0.06
		RMS1*	0.07	0.05	0.01	0.02	0.00	0.01	0.00
	Other	RMS2**	1.85	0.42	0.22	0.31	0.05	0.07	0.05

*RMS1 is Acc. RMS during "Time2" in the left column, while RMS2 corresponds to "Time1" in Table 2 excluded "Time2" here.
** RMS2 here corresponds to other times on 2011-2-22

Table 3: Structural Acc. Responses for Diff. Cases

Figure 17~Figure 19 are the power spectral density (PSD) plots of the vertical, lateral and torsional accelerations at the midspan, and CASE I is replotted in every subplot in each figure. For acceleration's sampling frequency is set to 50Hz, thus the cut-off frequency is 25Hz. Concentrating on the frequency range of 0~5Hz, some interesting phenomena could be seen from these figures. Firstly, the PSD of the acceleration induced only by the traffic loading increase by a larger amount in the frequency range of 2~5Hz than in the 0~2Hz by comparing CASE II with CASE I; secondly, acceleration's PSD induced only by the strong wind increased more obviously in the frequency range of 0~2Hz than 2~5Hz by comparing CASE III with CASE I, which is also found in [12]; and finally when acceleration is excited by both traffic and high winds, i.e. CASE IV, the frequency intervals 0~2Hz and 2~5Hz have similar increments in the acceleration PSD. It could be inferred that the exciting frequency of strong winds is lower than that of traffic.

The accelerations on the tower top and tower bottom have also been investigated. Figure 20 gives the PSD of acceleration response at the bottom of PM335, and the results also support the above inference on the frequency contents of high winds and traffic. In terms of CASE II, i.e. without high winds but with traffic, the traffic loading is only directly on the girder, the PSD in the upper subplot of Figure 20 demonstrates the vibration of the girder did affect the tower bottom. Although the vibration intensity caused by traffic is much lower than that in an earthquake, it is obviously different between CASE I and CASE II for the tower bottom vibration. Hence, it might not be appropriate to model the tower bottom as a fixed boundary when conducting dynamic analysis. Tabulated in Table 3 are the statistics of acceleration responses related to CASE I ~ CASE IV for a further comparison.

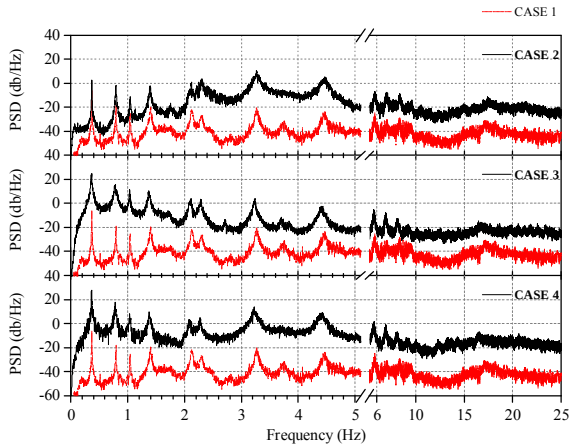

Figure 17: PSD of Vert. Acc. at the Midpoint

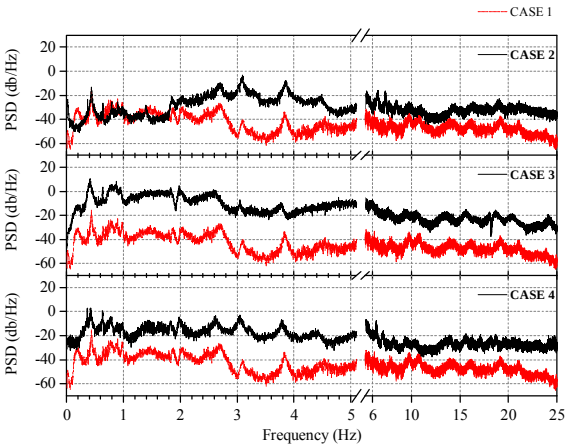

Figure 18: PSD of Lat. Acc. at the Midpoint

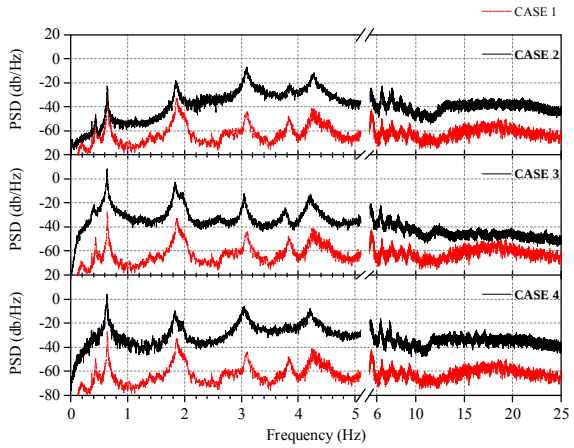

Figure 19: PSD of Tor. Acc. at the Midpoint

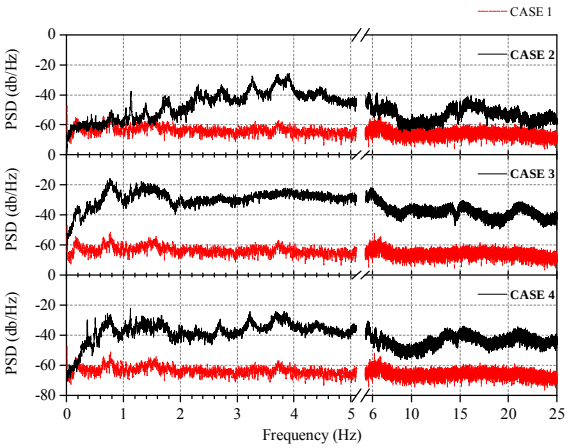

Figure 20: PSD of Lat. Acc. at Bot. of PM335

6 VARIATION OF MODAL PARAMETER DURING STRONG WINDS

Here, only the lower modes are considered. The frequencies and damping ratios of the 1st vertical bending, 1st lateral bending and 1st torsional modes are identified using Eigensystem Realization Algorithm (ERA) based on each of the 10-min acceleration data at the midspan. Figure 21~Figure 24 show the variation of modal parameters during 8-22 Gale and Typhoon Haikui, with the gray background meaning the high wind periods. Generally speaking, the modal frequencies become more scattered and in the meanwhile the damping ratios have an increasing tendency during high winds. The reason why the dynamic properties of the MNCB during high winds are so scattered might have something to do with the following facts:

- Structural stiffness, damping properties are not stable in high winds influenced by aero-dynamic effects;
- With exception of wind, modal parameters may also be affected by vibration intensity, structural temperature and so on;
- Measurement noise and algorithm errors coming from parameter identification process may also increase the uncertainty of the results.

Figures 25 and 26 are scatters of modal parameters versus wind speed, acceleration RMS and deck temperature during the bridge closure in Typhoon Haikui, where all the quantities are mapped to the interval [0, 1] and the wind speed is the component normal to the bridge axis. It appears that the modal parameters have a closer relation with the acceleration RMS, but other clear relations among these quantities are hard to be found. From the previous researches like [6, 9], the variation of modal parameters with regard to wind properties is also not so obvious, and the corresponding authors were cautious with their results as here.

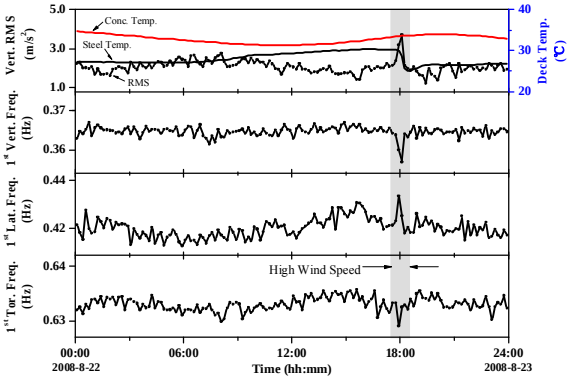

Figure 21: Modal Freq. on 2008-8-22 (1/2L)

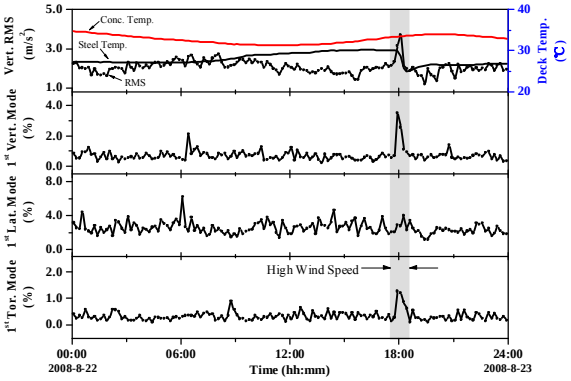

Figure 22: Damping Ratio on 2008-8-22 (1/2L)

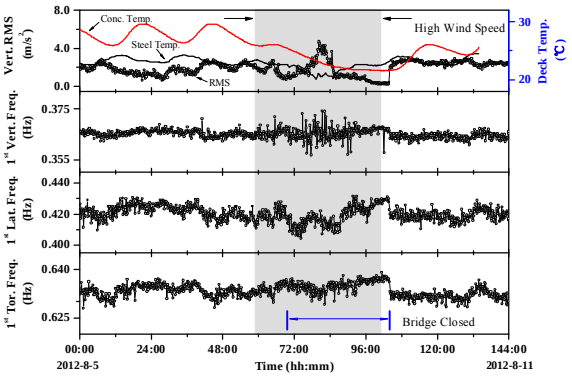

Figure 23: Modal Freq. during Haikui (1/2L)

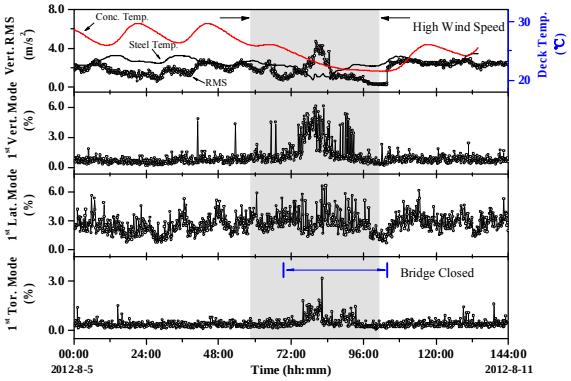

Figure 24: Damping Ratio during Haikui (1/2L)

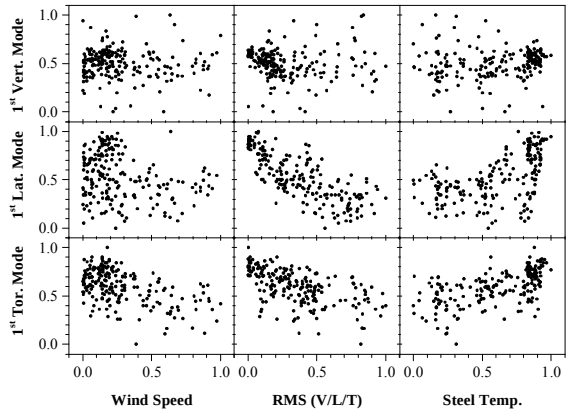

Figure 25: Freq. Vs Wind/RMS/Temp. during Haikui (1/2L)

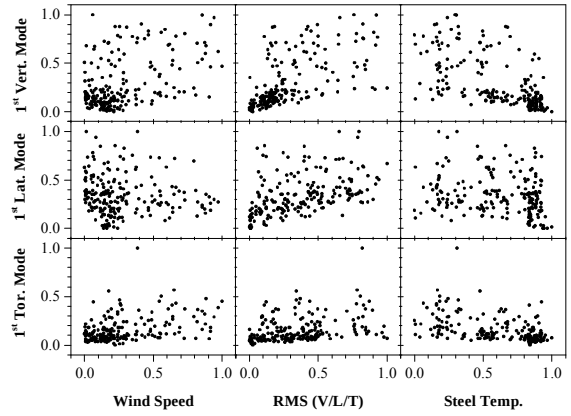

Figure 26: Damping Vs Wind/RMS/Temp. during Haikui (1/2L)

Additionally, there are two interesting phenomena that should be put forward. One comes from Figure 23, where modal frequencies drop by a relatively large amount at the end of bridge closure. This phenomenon demonstrates the influence of traffic loading on the modal frequency. The other phenomenon comes from Figure 17~Figure 19, where the higher modal frequencies also shift clearly to the lower side during CASE III and CASE IV. It should be kept in mind that CASE I and CASE II happened in the February, thus at low temperature, while CASE III and CASE IV happened in the August, with high temperature. Hence, the frequencies' decrease here may be attributed to the temperature's increase.

7 SUMMARY

Based on the field monitoring data from SHMS on the MNCB of Donghai Bridge, this paper investigates the wind field on site, and the wind effects in terms of structural acceleration responses and modal parameter's variation. Here some conclusions could be drawn as following:

1) About the Wind Environment: firstly, learned from the measurements, the wind field on the MNCB's site has a good repetition by one-year, and it is reasonable and possible to obtain the wind's probability density function by statistic approach; secondly, the measured wind characteristics could not be well represented by the assumption during the design stage, which indicates the importance and necessity of the feed-back from the field measurement to the design; thirdly, when the wind field is non-stationary, e.g. the wind direction changes dramatically, it is better to adopt a shorter average time duration than 10 minutes, or use a time-varying mean wind speed model; last but not least, the measured wind records on site might be disturbed by the structure. When making use of wind data from SHMS, it is necessary to consider the interference from the structure, e.g. directional effects;
2) About the Wind Effects on Structural Dynamic Responses: first of all, the strong winds and the traffic loading have different effects on the girder's vibration, at least for the MNCB of Donghai Bridge: the vertical and torsional vibrations depend more on the traffic loading while the lateral vibration are more sensible to the wind. In addition, wind loading has lower frequency contents than the traffic loading; secondly, under the operational conditions for a cable-stayed bridge, the vibration of the girder could be transferred to the bottom of the tower considerably, so it seems not to be so appropriate to take the bottom of the tower as a fixed point when performing dynamic analysis;
3) About the Wind Effects on Structural Modal Parameters: during high winds, the structural damping ratios have an increasing trend, and the modal frequencies become scattered, which might be caused by the structure's instability, other environmental or operational conditions, measurement noise and algorithm errors, etc... After each strong wind, the modal parameters of the MNCB could return to the stable and normal values, suggesting its good condition.

As a preliminary work, this paper inevitably has some shortcomings; and a further research concerning wind's effects on structures is required. Comments and suggestions would be welcome.

ACKNOWLEDGEMENT

The authors would extend great thanks to the financial support by the Research Program of State Key Laboratory of Disaster Reduction in Civil Engineering, Tongji University (Grand No. SLDRCE084-A-05), and the help from Shanghai Donghai Bridge Management Co., LTD as well as Shanghai Just One Technology Development Co., LTD.

REFERENCES

[1] Cross E J, Koo K Y, Brownjohn J M W, et al, Long-term monitoring and data analysis of the Tamar Bridge. *Mechanical Systems and Signal Processing*, 35(1–2), 16-34, 2013.

[2] Sohn H, Effects of environmental and operational variability on structural health monitoring. *Philosophical Transactions of the Royal Society A-Mathematical Physical and Engineering Sciences*, 365(1851), 539-560, 2007.

[3] Cury A, Cremona C, Dumoulin J, Long-term monitoring of a PSC box girder bridge: Operational modal analysis, data normalization and structural modification assessment. *Mechanical Systems and Signal Processing*, 33(0), 13-37, 2012.

[4] Joseph A M, Nicholas P J, A Comparison of Full-Scale Measurements of Stay Cable Vibration. Advanced Technology in Structural Engineering, Elgaaly M eds. *Structures Congress 2000-ASCE*, Philadelphia, USA, May, 2000.

[5] Fujino Y, Vibration, control and monitoring of long-span bridges—recent research, developments and practice in Japan. *Journal of Constructional Steel Research*, 58(1), 71-97, 2002.

[6] Abe M, Fujino Y, Yanagihara M, et al, Monitoring of Hakucho Suspension Bridge by ambient vibration measurement. Nondestructive Evaluation of Highways, Utilities, and Pipelines IV, Aktan A E, Gosselin S R eds. *SPIE 3995*, Newport Beach, CA, USA, March, 2000.

[7] Xu Y L, Zhu L D, Buffeting response of long-span cable-supported bridges under skew winds. Part 2: case study. *Journal of Sound and Vibration*, 281(3–5), 675-697, 2005.

[8] Xu Y L, Guo W W, Chen J, et al, Dynamic Response of Suspension Bridge to Typhoon and Trains. I: Field Measurement Results. *Journal of Structural Engineering*, 133(1), 3-11, 2007.

[9] Chen J, Xu Y L, Zhang R C, Modal parameter identification of Tsing Ma suspension bridge under Typhoon Victor: EMD-HT method. *Journal of Wind Engineering and Industrial Aerodynamics*, 92(10), 805-827, 2004.

[10] Wang H, Li A, Guo T, et al, Comparable study on typhoon and strong northern wind characteristics of the Runyang Suspension Bridge based on field tests. *Journal of Southeast University (English Edition)*, 25(01), 99-103, 2009.

[11] Min Z, Probabilistic analysis of condition properties of cable-stayed bridge based on long-term structural health monitoring. *Doctoral Dissertation of Tongji Univ.*, Shanghai, P.R.China, 2009.

[12] Min Z, Sun L, Dan D, Analysis of Wind-induced Response and Dynamic Properties of Cable-stayed Bridge Under Typhoon. *Journal of Tongji University (Natural Science)*, 37(9), 1139-1145, 2009.

[13] Brownjohn J M W, Zasso A, Stephen G A, et al, Analysis of experimental data from wind-induced response of a long span bridge. *Journal of Wind Engineering and Industrial Aerodynamics*, 54 – 55(0), 13-24, 1995.

[14] Miyata T, Yamada H, Katsuchi H, et al, Full-scale measurement of Akashi – Kaikyo Bridge during typhoon. *Journal of Wind Engineering and Industrial Aerodynamics*, 90(12 – 15), 1517-1527, 2002.

[15] Zuo D, Jones N P, Interpretation of field observations of wind- and rain-wind-induced stay cable vibrations. *Journal of Wind Engineering and Industrial Aerodynamics*, 98(2), 73-87, 2010.

[16] Ni Y Q, Wang X Y, Chen Z Q, et al, Field observations of rain-wind-induced cable vibration in cable-stayed Dongting Lake Bridge. *Journal of Wind Engineering and Industrial Aerodynamics*, 95(5), 303-328, 2007.

[17] Delaunay D, Grillaud G, Field measurements of the wind-induced response of a cable stayed bridge: Validation of previsional studies. *Journal of Wind Engineering and Industrial Aerodynamics*, 74 – 76(0), 883-890, 1998.

[18] Sun L, Sun Z, Dan D, et al, Large-span bridge and their health monitoring systems in China. In *Proceedings of 2007 International Symposium on Integrated Life-Cycle Design and Management of Infrastructure*, Shanghai, China, 2007.

[19] Zhu Z, Wind-induced responses research on main navigational channel bridge of Donghai Bridge. *Master's Thesis of Tongji Univ.*, Shanghai, P.R.China, 2007.

[20] Huang R, A Sea-Crossing's Design and Construction: Donghai Bridge, 1st Edition. China Communications Press, 2009.

[21] Xu Y L, Zhan S, Field measurements of Di Wang Tower during Typhoon York. *Journal of Wind Engineering and Industrial Aerodynamics*, 89(1), 73-93, 2001.

[22] Ministry of Transport of the People's Republic of China, *Wind-resistent Design Specification for Highway Bridges (JTG/T D60-01—2004)*. Beijing: China Communications Press, 2004.

[23] Holmes J D, *Wind Loading of Structures*, 1st Edition. Spon Press, 2001.

[24] Zhang X, Structural Wind Engineering: Theory, Code and Practice, 1st Edition. China Architecture & Building Press, 2006.

[25] Xu, Y, Chen J, et al, Occurrence probability of Wind-Rain-Induced stay cable vibration. *Advances in Structural Engineering*, 11(1), 53-69, 2008.

[26] The Water Resources Department of Fujian Province of P.R.China, Website of the water resource information system of Fujian Province, http://www.fjwater.gov.cn:8089, Nov, 2012.

[27] Xu Y, Chen J, Characterizing nonstationary wind speed using empirical mode decomposition. *Journal of Structural Engineering*, 130(6), 912-920, 2004.